Available online at www.sciencedirect.com
ScienceDirect
Acta Materialia 57 (2009) 4765–4772
Acta MATERIALIA
www.elsevier.com/locate/actamat

Oxygen vacancy diffusion in alumina: New atomistic simulation methods applied to an old problem

U. Aschauer [a,*], P. Bowen [a], S.C. Parker [b]

[a] *Laboratoire de Technologie des Poudres, EPFL, Lausanne, Switzerland*
[b] *Department of Chemistry, University of Bath, Bath, UK*

Received 19 December 2008; received in revised form 18 June 2009; accepted 23 June 2009
Available online 27 July 2009

Abstract

Understanding diffusion in alumina is a long-standing challenge in ceramic science. The present article applies a novel combination of metadynamics and kinetic Monte Carlo simulation approaches to the investigation of oxygen vacancy diffusion in alumina. Three classes of diffusive jumps with different activation energies were identified, the resulting diffusion coefficient being best fitted by an Arrhenius equation having a pre-exponential factor of 7.88×10^{-2} m^2 s^{-1} and an activation energy of 510.83 kJ mol^{-1}. This activation energy is very close to values for the most pure aluminas studied experimentally (activation energy 531 kJ mol^{-1}). The good agreement indicates that the dominating atomic-scale diffusion mechanism in alumina is vacancy diffusion.

Keywords: Crystalline oxides; Bulk diffusion; Molecular dynamics simulations; Monte Carlo simulations

1. Introduction

In order to improve ceramic materials such as alumina (α-Al_2O_3) and obtain the very specific properties required for novel high-performance applications, a fine control over the microstructure is required. This requires in turn a fundamental understanding of sintering, the underlying atomic-scale diffusion mechanisms of the constituent oxygen anions and aluminium cations, and how these mechanisms are influenced by the presence of dopants. Despite many years of intensive research on diffusion in alumina these mechanisms are still the subject of much speculation, as reviewed recently by Doremus [1] and Heuer [2]. Since experimental investigations of a specific diffusion mechanism are very difficult to carry out, simulations are a promising way to gain the required understanding of diffusion at an atomistic scale.

It is generally admitted that oxygen diffusion is lower than aluminium diffusion under all conditions and will thus be rate limiting. In his review articles [2,3] Heuer points out that the experimental studies on oxygen diffusion in nominally undoped alumina are in rather good agreement, the scattering being within one order of magnitude. He also notes, however, that theoretical studies have so far not been able to elucidate the atomic mechanism behind diffusion processes. The theoretically calculated migration energies are of the order of 1–2.5 eV [1,2], whereas experiment [3] gives migration energies of the order of 5 eV. This discrepancy is so far unexplained, though a controversial mechanism was published by Doremus [1], who suggested that the possible presence of AlO bivacancies may be able to better account for such discrepancies.

The formation of oxygen vacancies by intrinsic Schottky and Frenkel defects has been studied by many authors [4–9] using computational methods. The reported formation energies per defect for the Schottky defect range from 4.18 to 5.86 eV and from 3.79 to 8.27 eV for the anion Frenkel defect. The relatively high variability of defect energies is attributed to the different interatomic potentials

* Corresponding author. Present address: Department of Chemistry, Princeton University, Princeton, NJ, USA.
E-mail address: uli.aschauer@epfl.ch (U. Aschauer).

1359-6454/$36.00 © 2009 Acta Materialia Inc. Published by Elsevier Ltd. All rights reserved.
doi:10.1016/j.actamat.2009.06.061

and computational methods used in the theoretical approaches. These relatively high formation energies will result in a small population of defects and the comparable formation energies make it difficult to determine the dominant oxygen vacancy formation mechanism [10]. Oxygen vacancies may also be formed as charge-compensating defects when aliovalent dopants are present – though this is beyond the scope of the present paper, which looks at undoped alumina only.

To date, the most complete theoretical study on anion migration has been carried out by Jacobs and Kotomin [5], who used an empirical potential method to identify five possible migration paths in the unit cell. Their saddlepoint determination procedure is not well documented but seems to be by interpolation between discrete ion positions. Jumps are classified to be in "small" triangles, located in between two octahedral aluminium ions and "large" triangles in the vicinity of an octahedral interstitial site. They found very low migration energies (0.34 eV) within the small triangle and a higher one (2.5 eV) in the large triangle. Migration between the triangles is possible by paths with energies of 1.85 and 1.37 eV. There is a fifth migration path with an activation energy of 5.1 eV, but no geometric information is given as the authors do not consider this jump to be of any importance. Jacobs and Kotomin finally suggest two diffusion paths having limiting activation energies of 2.5 and 1.85 eV, respectively. They compare their results to an experiment by Oishi and Kingery [11] and report an "excellent" agreement. It has, however, to be noted that the activation energy reported by Oishi and Kingery to which they compare their theoretical calculations is an "extrinsic" activation energy. According to Oishi and Kingery this corresponds to "impurity or structure sensitive diffusion" and is significantly different to the intrinsic calculations they performed which were for pure alumina. The same authors [6] published semi-empirical calculations of the same migration energies, which showed significant variations for the "small" triangle jumps (+0.15 eV compared to the empirical calculations) and the one of the inter-triangle migrations (+1.65 eV compared to the empirical calculations). More recently vacancy migration has been calculated using density functional methods [12] and a migration energy of 3.7 eV for the lowest energy jump has been obtained. This jump seems to be within a small closed triangular path, whereas the migration energies for the other jumps are unfortunately not given.

In summary these simulations cannot satisfactorily explain oxygen diffusion mechanisms at an atomic scale that are in agreement with experimental results. The experimental measurements of diffusion coefficients are themselves fraught with difficulties both in the determination of impurity concentrations [2] and data evaluation [1]. In his second review [2] Heuer therefore formulates a series of open questions related to diffusion in alumina. The majority of these questions are linked to anion diffusion, touching areas such as the significance of experimental activation energies, the nature of the buffering that seems to occur in oxygen diffusion, the diffusion mechanisms, as well as the ratios between anion and cation diffusion in the bulk and grain boundaries. For better interpretation of data and a deeper understanding of the basic diffusion mechanisms, a better model at the atomistic level is needed.

The present study applies a novel simulation approach based on empirical potential-based metadynamics (MTD) and kinetic Monte Carlo (kMC) methods to the investigation of oxygen vacancy diffusion in alumina. This technique has the advantage of being able to deduce migration free energies for individual diffusive jumps and then use these to determine macroscopic diffusion coefficients through the kMC method.

2. Methods

The techniques used in the present work are MTD [13–15] and kMC, which have been used separately in the literature [16,17] for this type of diffusion calculation. In MTD one defines one or more so-called collective variables (CVs), which allow us to differentiate between the states of interest of the system. These can be interatomic distances, angles, coordination numbers or any other property definable in terms of the atom positions. The MTD technique is very useful in studying systems with deep local minima separated by high potential energy barriers. Transitions between these minima are made possible within the simulation timescale by using a history-dependent bias potential constructed by summing Gaussian contributions of height h_h and width h_w in the space defined by the CV as follows:

$$V_{\text{bias}}(\vec{s},t) = h_h \sum_{i=1}^{n(t)} \exp\left(-\frac{(\vec{s}-\vec{s}_i)^2}{2(h_w)^2}\right), \tag{1}$$

where $\vec{s}$ is a point in CV space, t the simulation time and $\vec{s}_i$ the position in CV space of the ith CV. The number of steps $n(t)$ is determined by the simulation time and the insertion frequency of the bias contributions. The bias potential is then applied to all atoms defining the CV, giving them additional energy to overcome the free energy barriers. Moreover the method allows the underlying free energy surface to be determined, as the sum of all Gaussians is an unbiased estimator of the free energy [15].

For the present work, the method has been implemented in the empirical potential molecular dynamics code DL_POLY 2.0 [18]. Empirical potential codes have the advantage of being able to calculate larger structures such as low vacancy or dopant concentrations or near general grain boundaries, which would not be possible using existing first-principles MTD implementations due to the high number of atoms.

To prepare crystals for the MTD runs, a bulk supercell ($6 \times 6 \times 2$) of the hexagonal alumina unit cell [19] has been heated in steps of 100 K (100 ps each) using the NPT (variable volume) ensemble in the unmodified DL_POLY 2.0 code with Lewis and Catlow [20] pair potentials, which

are known to describe bulk, surfaces and grain boundaries in α-alumina with reasonable accuracy [21–23]. Table 1 gives the most important bulk properties calculated using the present potential and compares them to experimental values. As can be seen, except for a slight compression of the unit cell along the hexagonal *c*-axis, experimental values are reproduced reasonably well. Normally so-called "ab initio" methods are considered more accurate than empirical potentials even though the local density approximation and generalized gradient approximation exchange and correlation functionals used in modern density functional theory (DFT) calculations are known to over- and underbind for unphysical reasons and to completely neglect dispersion interactions [24]. As we recently showed by direct comparison with DFT calculated grain boundary structures in alumina [25], the potential results in structures with a maximum deviation of 0.3 Å with respect to the DFT coordinates. As the results compare well with respect to both experiment and DFT calculations, the empirical potential can be considered to describe the alumina lattice with good accuracy. Samples were extracted at 1, 300, 1100 and 1700 K. Parameters used for these simulations as well as the MTD runs were a time step of 0.0001 ps, a short-range cut-off of 10 Å and a Nose–Hoover thermostat as well as Hoover barostat with relaxation times of 0.5 ps. For each simulation run a single vacancy was generated and for all neighbouring oxygen ions (cut-off distance 3.1 Å) MTD calculations of the jump into the created vacancy position were performed. Runs were performed for all oxygen sites within one unit cell of the supercell. This may seem superfluous, as many of the jumps are equivalent due to the crystal symmetry, however, as will be seen later, a high number of runs were required for good statistical averaging. Charge balance was achieved by smearing the charge of the vacancy over the aluminium sublattice, resulting in a charge of 2.9977 on these ions. The small change and the isotropic nature of this modification should lead to negligible modifications of the electrostatic interactions in the system.

The CV for MTD runs was defined as the distance between the jumping and the position previously occupied by the ion removed to create the vacancy. Compared to alternative possibilities, such as coordination numbers or interatomic distances and angles, this CV setup has the advantage that a single CV can determine which atom is to jump, thus requiring only a one-dimensional CV space to be filled by the bias potential. The projection of this CV into real space is a sphere centred on the vacancy position (a certain CV value represents the union of all points at this distance from the vacancy position), meaning the bias potential added on one point of the sphere will also be applied in all other points of the spherical shell with the same radius. However, as the jumping atom will start far from the centre of the sphere and follow a single transition path out of its potential well, the sphere will be traversed in only one position. Once the atom is at the centre of the sphere, the CV setup will lead to ambiguities with respect to positioning in CV space, and the backwards reaction is not possible in the same run.

Since the structure will relax as a result of the vacancy creation, MTD was started only after 500 time steps, which was found to be sufficient for relaxation. Gaussian-shaped contributions of 80 J mol^{-1} height and 0.3 Å width were added to the bias potential every 20 time steps. Compared to similar MTD studies using semi-empirical methods [16], the height is about 60 times smaller, leading to a more precise filling of the underlying free energy surface.

MTD runs were stopped once the jumping atom reached the vacancy position and the free energy barrier separating the two minima calculated by locating the peak on the bias potential along the CV. The hopping rates for the kMC simulations were estimated from these barriers (ΔG_i) using transition state theory and more specifically Eyring's equation [26] (Eq. (2) below). Using the hypothesis that the partition functions for the vibrational states q_{vib} at lattice sites and at the saddlepoint are similar, the approximate version given on the right-hand side of Eq. (2) is obtained:

$$r_i = \frac{1}{2}\frac{q_{\mathrm{vib}}^{\mathrm{saddle}}}{q_{\mathrm{vib}}^{\mathrm{lattice}}}\frac{kT}{h}\exp\left(-\frac{\Delta G_i}{kT}\right) \approx \frac{1}{2}\frac{kT}{h}\exp\left(-\frac{\Delta G_i}{kT}\right). \qquad (2)$$

In this equation k is Boltzmann's constant, T the temperature and h Planck's constant. The ½ pre-factor is the transmission coefficient, taking into account that an atom having reached the saddlepoint has an equal probability of falling forward into the next free energy well or backward into the originating well. It should be noted [27] that from a strictly physical point of view Planck's constant would not appear in the relation for the rate constant as it cancels out with the h also appearing in the vibrational partition functions. The present use of Planck's constant as a conversion factor between energy and frequency is an ambiguous result of the approximation that the vibrational partition functions are similar for the lattice site and saddlepoint, which for tightly bound states such as in a bulk crystal is a reasonable assumption. Given the accuracy of the free energy barriers attainable using empirical potentials, more precise approaches for the evaluation of the partition functions, such as the harmonic transition

Table 1
Comparison between calculated and experimental properties of alumina: lattice constants a and c, dielectric tensor elements ε_{ii}, elastic tensor elements C_{ii} and potential energy U_{pot}.

Property	Experiment	Calculation
a (Å)	4.76	4.72
c (Å)	12.99	12.43
ε_{11} (–)	9.34	8.24
ε_{33} (–)	11.54	12.52
C_{11} (GPa)	497.35	666.09
C_{12} (GPa)	163.97	269.10
C_{13} (GPa)	112.20	191.59
C_{33} (GPa)	449.11	519.88
C_{44} (GPa)	147.39	157.96
U_{pot} (kJ mol^{-1})	−15916	−15533

state theory [28], are unlikely to yield a more accurate description of the system.

kMC simulations were carried out by randomly placing the vacancy on an oxygen site in the unit cell and then locating all possible transitions with nearest neighbours. The cumulative function was calculated as:

$$R_i = \sum_{j=1}^{i} r_j. \tag{3}$$

The transition i to be carried out was defined by a random number u uniformly distributed between 0 and 1 imposing $R_{i-1} < uR_n \leq R_i$, where n is the index of the last element of the cumulative function. The simulation time is advanced for each transition as given by Eq. (4), where v is another random number uniformly distributed between 0 and 1:

$$\Delta t = -\frac{\log v}{R_n}. \tag{4}$$

A slight modification of this standard kMC method was required in the present case for reasons to be described in Section 3.2, where the required modifications will be introduced as well.

kMC simulations were run for at least 500,000 jumps, and 100 runs per temperature were performed to obtain a reliable average. The temperatures looked at were 1400, 1600, 1800, 2000 and 2200 K, and are thus situated within the range of standard alumina sintering temperatures.

The mean square displacement (MSD) was calculated over all kMC runs as:

$$\mathrm{MSD}(t) = \langle |\vec{r}(t) - \vec{r}(0)|^2 \rangle, \tag{5}$$

where $\vec{r}(t)$ is the position of the vacancy at time t and the angle brackets denote an averaging over all runs. The diffusion coefficient D was finally deduced using Einstein's relation:

$$D = \lim_{t\to\infty} \frac{\mathrm{MSD}(t)}{6t}. \tag{6}$$

3. Results and discussion

3.1. Metadynamics calculations

The minimum migration energies calculated over all samples at each temperature (1, 300, 1100 and 1700 K) are reported in Fig. 1 as a function of the jump distance in the 1 K structure. As can be seen, there are three distinct groups of jumps corresponding to very specific interatomic distances in the low-energy structure. Jumps of lowest energy are the shortest and have migration free energies of about 1.5–3.0 eV at low temperatures, an increase in temperature leading to a decrease and a widening of the migration energy distribution. The medium distance class of jumps has very high migration free energies of the order of 7–9 eV at low temperature, an increase in temperature again lowering the energy but also leading to a larger distribution of values. The same is also observed for the class of longest jumps, which has activation free energies of 5–6 eV at low temperature. In the following these jumps will be referred to as jumps belonging to classes 1, 2 and 3, ranked by increasing distance. The scatter of values, which is rather large even for the 1 K case, comes from the fact that close to the transition state the amount of energy inserted by the hills is significant with respect to the changes in the underlying free energy surface. This leads to a loss in precision in determining the exact free energy barrier, depending on the position in CV space, where the hill is inserted. Techniques such as adaptive hills as implemented in the CPMD code [29] could help to improve this limitation.

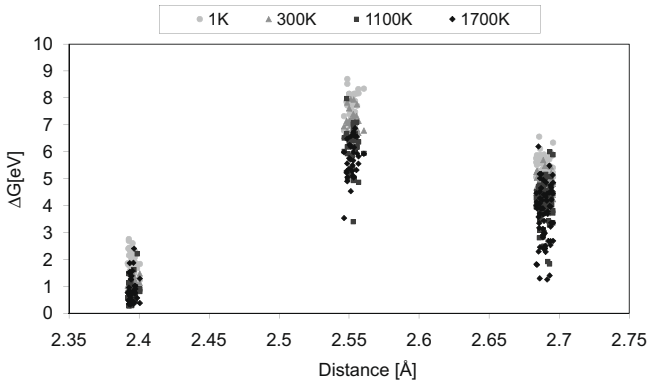

Fig. 1. Migration energies for 1300, 1100 and 1700 K as a function of the jump distance at 1 K.

It would seem that the previously reported migration energies [5,30] were of class 1; however, the highest energy reported without geometric information by Jacobs and Kotomin [5] is most likely part of class 3. Although the jump calculated using DFT methods [12] seems to be of class 1 according to the geometrical information given by Carrasco et al. [12], it has an activation energy in between those of jumps belonging to classes 1 and 3 of the present work. It is not clear if this is a result of the method (constrained search vs. MTD) or the energy calculation (DFT vs. empirical potentials). Methods such as a transition state search would locate the lowest saddlepoint energies only, which are jumps represented by class 1. This shows the clear advantage of the present approach, which systematically probes jumps between all pairs of sites in the structure, thus giving a more complete picture.

Fig. 2 shows a typical transition path of a neighbouring oxygen ion (a series of semitransparent spheres) to the vacancy position. As can be seen, the transition path is not linear: the jumping ion swings around the nearest aluminium ion. Jacobs and Kotomin probed both linear and curved transition paths, rejecting the latter due to higher saddlepoint energies. Compared to their method, the present approach has the advantage of not imposing a path but letting the system locate the lowest saddlepoint, thus finding the most favourable transition path. This suggests that the transition path is in fact curved but complex and thus

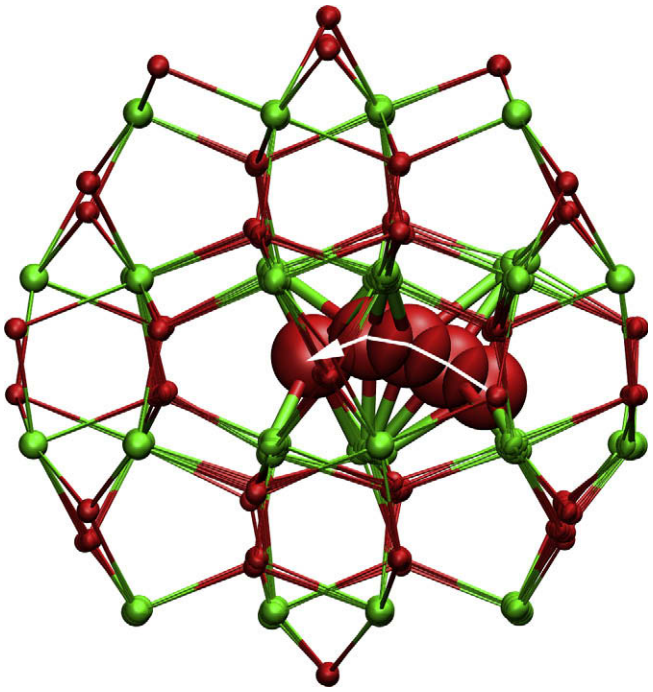

Fig. 2. Typical transition path of a neighbouring oxygen ion (series of semitransparent spheres) to a vacancy position (green sphere) within the alumina lattice (aluminium = ochre nodes, oxygen = red nodes). (For interpretation of the references to colour in this figure legend, the reader is referred to the web version of this article.)

not easily guessed. The non-linearity could be one of the main reasons for the slight differences in migration free energies compared to previous studies.

The distributions of the jumps of the three classes within the hexagonal alumina unit cell are shown in Fig. 3. The low-energy jumps of class 1 are found in triangles located in the mid-plane between two adjacent aluminium ions, which is in agreement with the results by Jacobs and Kotomin [5]. It can be seen that there is no connection between the low-energy diffusive jumps in this class, the vacancy remaining within the triangle when only this class of jumps is active. The second class of jumps being of the highest energy forms three linear but not interconnected diffusion paths, whereas the third class forms an interconnected network. This data shows that the low-energy jumps, previously predicted and simulated, do not contribute to the macroscopic diffusion coefficient as they only allow migration of the vacancy within the small triangles. This non-continuity was one of the hypotheses put forward by Harding et al. [31], and is now confirmed by the present results and may explain the discrepancy between simulation and experimental migration energies pointed out by Heuer [2]. The next lowest energy class is the third one, which due to its interconnected nature is expected to be the diffusion-dominating class. The second class, being of such high energy, is expected to play a minor role.

Plotting the mean value of the energy clouds in Fig. 1 as a function of temperature yields the graph shown in Fig. 4. The error bars shown represent the standard deviation within the cloud of jumps. In traditional diffusion theory the activation energy is often assumed not to vary with temperature. The present results, however, show a variation that can be attributed to the additional kinetic energy provided to the jumping atoms due to the vibration of its neighbours. The migration free energy is expected to follow

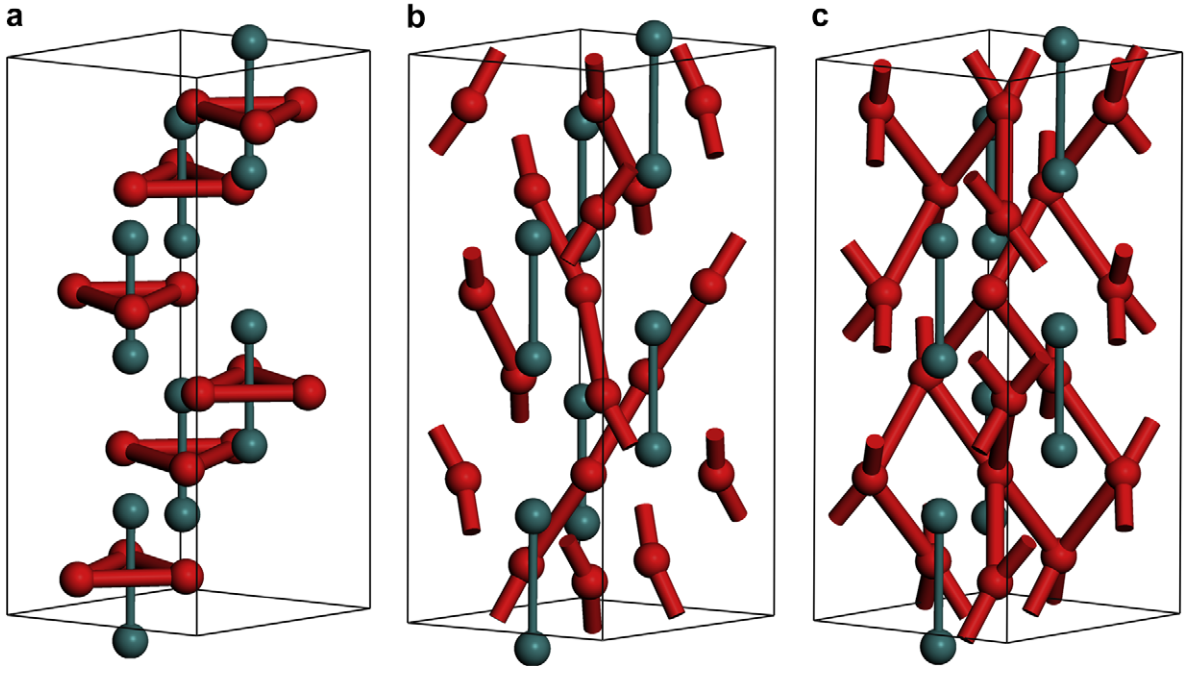

Fig. 3. Distribution of oxygen vacancy jumps in the alumina unit cell (aluminium = green, oxygen = red) shown by red bonds for: (a) class 1, (b) class 2 and (c) class 3. (For interpretation of the references to colour in this figure legend, the reader is referred to the web version of this article.)

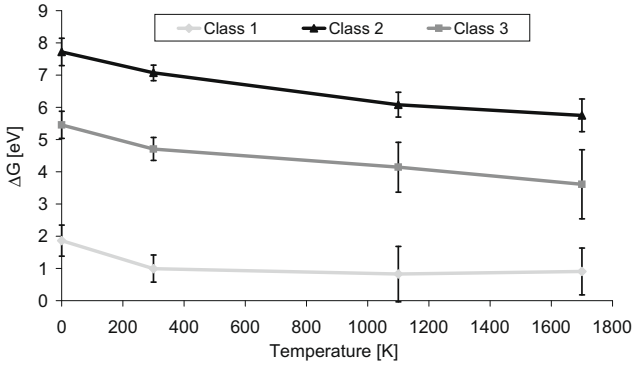

Fig. 4. The average jump energies per class as a function of temperature.

a temperature (T)-dependent law of the form given by Eq. (7), containing both enthalpy (ΔH) and entropy (ΔS) terms:

$$\Delta G_{\text{migration}}(T) = \Delta H_{\text{migration}} - T\Delta S_{\text{migration}}. \quad (7)$$

A linear fit of the data shown in Fig. 4 would, however, only be acceptable for classes 2 and 3. For this reason the discrete data points were used to deduce migration free energies at different temperatures for the kMC simulations, using linear interpolation between points and linear extrapolation at higher temperatures.

3.2. Kinetic Monte Carlo calculations

The large difference in migration free energies would, according to Eq. (2), result in about 10^7 class 1 jumps in between each two class 3 jumps. A standard kMC implementation would thus be extremely inefficient since a high number of class 1 jumps, which do not contribute to diffusion, have to be carried out in order to get a good statistical average of class 3 jumps. It was therefore decided to alter the kMC method as follows to implicitly include class 1 jumps. The series of class 1 jumps will result in the vacancy migrating from one site in the triangle to another (or the same) site. This process can thus be described by placing the vacancy randomly on one of the triangle sites. The time step associated with this process can be written as given by Eq. (8), where r_{fast} is the rate of the fast class of jumps, Δt_{last} is the time step of the last slow jump, and u a random number between 0 and 1:

$$\Delta t = r_{\text{fast}}\Delta t_{\text{last}}\frac{1}{r_{\text{fast}}}2u = \Delta t_{\text{last}} \cdot 2u. \quad (8)$$

It can be seen that the first two factors express the number of fast jumps, the third gives the time step of a fast jump, and the last takes into account the stochastic nature of the process by multiplying the number of steps by a random number centred on 1. Simulations carried out in this way result in random vacancy migration paths, an example of which projected into the crystallographic a–c plane is shown in Fig. 5.

It is worth emphasizing that we are modelling extrinsic diffusion where existing defects are responsible for atom

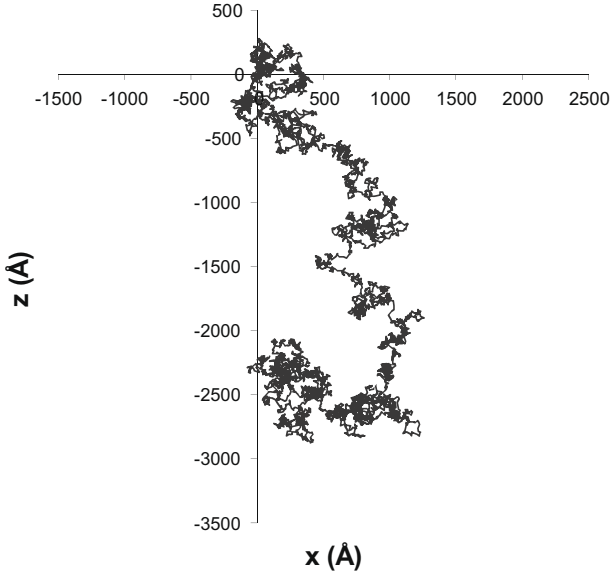

Fig. 5. Example vacancy migration path projected into the crystallographic a–c plane.

transport, and hence the activation energy for diffusion depends only on the migration energy. In contrast, intrinsic diffusion is dependent on the sum of the formation and migration energies. At the temperatures considered in this work (1400–2200 K), intrinsic diffusion will not be significant, as can be illustrated by looking at the defect formation energies. The formation energy for an oxygen vacancy is known to be about 5 eV per defect for either Frenkel or Schottky disorder [4–9]; the potentials used in the present work predict the lowest energy to be the Frenkel defect with 4.6 eV per defect. This means that in the temperature range of interest (1400–2200 K) the atomic fraction of intrinsic vacancies is of the order of 10^{-17}–10^{-11}. If one of the purest materials possible in experiments (0.1 ppm Mg) is considered, the atomic fraction of charge-compensating vacancies that would have to be present would be 0.05 ppm $= 5 \times 10^{-8}$. The concentration of impurity-induced vacancies is therefore at least three orders of magnitude larger than those created intrinsically, and oxygen vacancy diffusion can be assumed to be dominated by extrinsic vacancies in the considered temperature range. Even though impurities and other oxygen vacancies are present in the extrinsic diffusion regime, their concentration is so low that their average population in the considered simulation box would be well below one atom. As a first approximation the present simulation cell without the presence of these defects can therefore be considered a good representation of an experimental system.

Plotting the MSD as a function of time for different numbers of runs gives the graph shown in Fig. 6. It can be seen that whereas for one run the oscillations are still significant, after only 10 runs the graph approaches its final slope. Hundred runs result in clear trends, whereas for 1000 runs an almost straight line is obtained. This shows that in

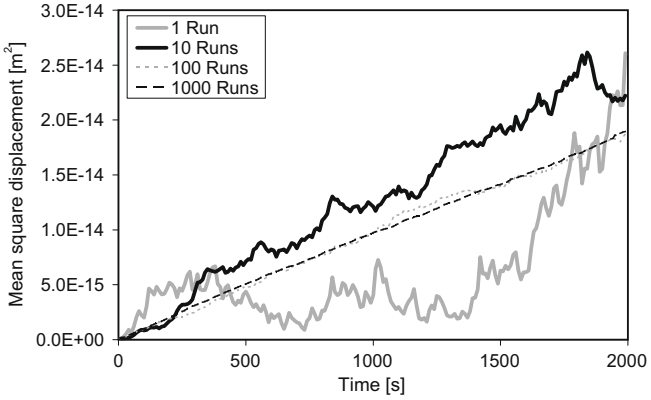

Fig. 6. The mean squared displacement as a function of time for 1, 10, 100 and 1000 runs.

the present case 100 runs should be enough to obtain a good statistical average.

The mean square displacements for temperatures between 1400 and 2200 K obtained using this method are plotted in Fig. 7. The diffusion coefficient at a certain temperature is deduced according to Eq. (6) by dividing the slope of each linear trend line by six. If one finally plots the diffusion coefficient as a function of the inverse temperature, the plot shown in Fig. 8 is obtained. It can be seen that an almost straight line is obtained, showing the good statistical averaging obtained in the kMC simulations. This data can be fitted to an Arrhenius equation with a pre-exponential factor of $7.88 \times 10^{-2}\ m^2\ s^{-1}$ and an activation energy of 510.83 kJ mol^{-1}.

The activation energy is slightly lower but of the same order of magnitude as those summarized in the reviews of Doremus [1] and Heuer [2], which are reported in Table 2 together with the most relevant impurities. From Table 2 it seems that there is a tendency of decreasing activation energy with increasing purity of the material, especially visible in the recent work by Ikuhara and co-workers [32,33]. Impurities will influence the energy landscape by interaction with oxygen vacancies by electrostatic and van der Waals type forces as well as by misfit strains in the lattice,

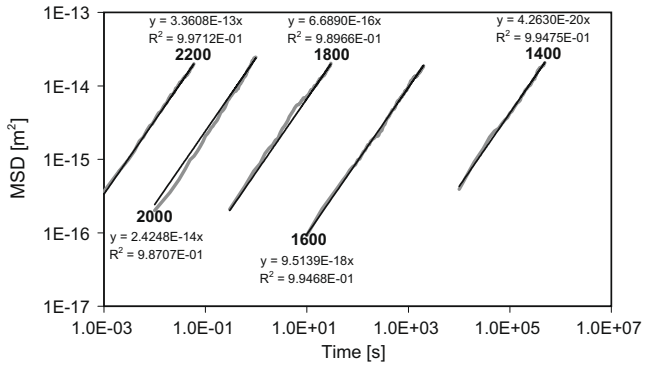

Fig. 7. Mean square displacement as a function of time for different temperatures.

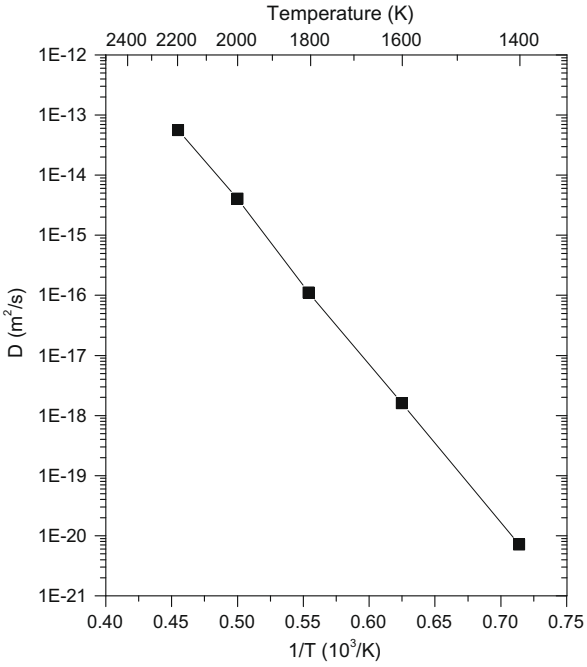

Fig. 8. Diffusion coefficient as a function of the inverse temperature.

changing activation energies and giving a possible explanation for the fact that the activation energies in the perfectly pure simulated crystal are lower than experimental ones. Vacancy–impurity interaction and its effect on vacancy migration is, however, far from trivial, and its study will be an interesting future application of the present method. However, given the fact that the activation energy is roughly the same as found experimentally, it seems reasonable to assume that the simulations describe the experimentally relevant diffusion mechanism.

The present study looks at the diffusion of vacancies and not the resulting diffusion of oxygen ions. Since, to our knowledge, no suitable theory correlating the jumps of these two entities exists for the alumina lattice, comparison of the pre-exponential factors with those measured by tracer diffusion experiments is at this time not possible. Future kMC studies based on the present work should, however, also be able to numerically determine ion diffusion coefficients.

This good agreement with experimental activation energies gives strong support to the atomic-scale diffusion mechanism found using the MTD calculations. This elucidates the long-standing problem of oxygen diffusion in alumina, and provides an explanation for the disagreement between previous theoretical studies and experiment. The present method has the advantage over previous studies that it does not restrict the transition path in any way, thus allowing the system to locate the lowest energy saddle-point. The method developed here will allow further study of a manifold of diffusion mechanisms in alumina and other ceramics, opening the way to understanding of diffusive phenomena in the solid state. Possible future research using the present approach include looking at ion diffusion

Table 2
Summary of previous experimental results from the literature.

Refs.	Q (kJ mol^{-1})	D_0 (m^2 s^{-1})	Impurities (ppm)						
			Na	Mg	Ca	Fe	Si	Ti	Others
[32]	531	2.9×10^{-1}	<1	<0.1	<0.1	<1		2.8	K < 1, Ba < 0.1, Zn < 1, Mo < 6, W < 6, Mn < 0.2, Cd < 2
[33]	562	2.4×10^{-4}	4	3	5	1	3	<0.5	K = 3
[34]	572	1.5×10^{-3}							Unspecified: 80–100
[35]	589 ± 19	6.8×10^{-4}	<12	<2	<4	<4	<6	<4	As < 283, B < 6, Cr < 6, Mo < 13, Ni < 6, P < 98, Pb < 54, Sb < 66, Se < 65, Sn < 20, V < 4
[36]	615 ± 40	2.7×10^{-2}		5	26	16	60	4	Sn = 66
[37]	636 ± 20	2.1×10^{-2}		63	382	14	817		
[38]	665	5.6×10^{-2}				5	10		
[39]	787 ± 29	6.4×10^{1}		<1		9	11		Cu < 1

coefficients, other mechanisms such as interstitial diffusion, the interaction of diffusing species with dopants, and diffusion in grain boundaries.

4. Conclusions

Oxygen vacancy diffusion in alumina was investigated using a combination of MTD and kMC simulation methods. It was found that using MTD simulations resulted in three distinct classes of diffusion jumps in alumina, although the lowest energy one does not contribute to bulk diffusion as they do not form a continuous network. The next highest energy class forms such a network and is thus the diffusion-dominating class. kMC simulations using these migration free energies resulted in vacancy diffusion coefficients that reproduce experimental activation energies very well, thus validating the present approach. The present data shows that the dominating atomic-scale diffusion mechanism in alumina is based on vacancy migration. The approach is generic and can now be applied to other structural elements of the alumina system (such as grain boundaries) as well as other ceramic materials.

Acknowledgement

This work was financially supported by the European Sixth Framework Integrated Project Nanoker No. NMP3-CT-2005-515784.

References

[1] Doremus RH. J Appl Phys 2006:100.
[2] Heuer AH. J Eur Ceram Soc 2008;28:1495.
[3] Heuer AH, Lagerlöf KPD. Philos Mag Lett 1999;79:619.
[4] Catlow CRA, James R, Mackrodt WC, Stewart RF. Phys Rev B 1982;25:1006.
[5] Jacobs PWM, Kotomin EA. Philos Mag A 1993;68:695.
[6] Jacobs PWM, Kotomin EA. J Solid State Chem 1993;106:27.
[7] Grimes RW. J Am Ceram Soc 1994;77:378.
[8] Lagerlöf KPD, Grimes RW. Acta Mater 1998;46:5689.
[9] Atkinson KJW, Grimes RW, Levy MR, Coull ZL, English T. J Eur Ceram Soc 2003;23:3059.
[10] El-Aiat MM, Kröger FA. J Am Ceram Soc 1982;65:162.
[11] Oishi Y, Kingery WD. J Chem Phys 1960;33:480.
[12] Carrasco J, Lopez N, Illas F. Phys Rev Lett 2004:93.
[13] Laio A, Parrinello M. Proc Natl Acad Sci USA 2002;99:12562.
[14] Iannuzzi M, Laio A, Parrinello M. Phys Rev Lett 2003:90.
[15] Laio A, Rodriguez-Fortea A, Gervasio FL, Ceccarelli M, Parrinello M. J Phys Chem B 2005;109:6714.
[16] Jug K, Nair NN, Bredow T. Phys Chem Chem Phys 2005;7:2616.
[17] Krishnamurthy R, Yoon YG, Srolovitz DJ, Car R. J Am Ceram Soc 2004;87:1821.
[18] Smith W, Forester TR. J Mol Graph 1996;14:136.
[19] Liu RS, Shi WC, Cheng YC, Huang CY. Mod Phys Lett B 1997;11:1169.
[20] Lewis GV, Catlow CRA. J Phys C 1985;18:1149.
[21] Davies MJ, Kenway PR, Lawrence PJ, Parker SC, Mackrodt WC, Tasker PW. J Chem Soc–Faraday Trans 2 1989;85:555.
[22] de Leeuw NH, Parker SC. J Am Ceram Soc 1999;82:3209.
[23] Baudin M, Hermansson K. Surf Sci 2001;474:107.
[24] Coquet R, Howard KL, Willock DJ. Theory: periodic electronic structure calculations. In: Jackson SD, Hargreaves JSJ, editors. Metal oxide catalysis, vol. 1. Weinheim: Wiley-VCH; 2008. p. 323.
[25] Galmarini S, Aschauer U, Bowen P, Parker SC. J Am Ceram Soc 2008;91:3643.
[26] Eyring H. J Chem Phys 1935;3:107.
[27] Voter AF. Introduction to the kinetic Monte Carlo method. In: Sickafus KE, Kotomin EA, editors. Radiation effects in solids. Dordrecht: Springer, NATO Publishing Unit; 2005.
[28] Vineyard GH. J Phys Chem Solids 1957;3:121.
[29] CPMD. Copyright IBM Corp. 1990–2006, Copyright MPI für Festkörperforschung Stuttgart1997–2001.
[30] James R. PhD Thesis, University of London; 1978.
[31] Harding JH, Atkinson KJW, Grimes RW. J Am Ceram Soc 2003;86:554.
[32] Nakagawa T, Nakamura A, Sakaguchi I, Shibata N, Lagerlöf KPD, Yamamoto T, et al. J Ceram Soc Jpn 2006;114:1013.
[33] Nakagawa T, Sakaguchi I, Shibata N, Matsunaga K, Mizoguchi T, Yamamoto T, et al. Acta Mater 2007;55:6627.
[34] Cawley JD, Halloran JW, Cooper AR. J Am Ceram Soc 1991;74:2086.
[35] Lagerlöf KPD, Mitchell TE, Heuer AH. J Am Ceram Soc 1989;72:2159.
[36] Reddy KPR, Cooper AR. J Am Ceram Soc 1982;65:634.
[37] Prot D, Monty C. Philos Mag A 1996;73:899.
[38] Oishi Y, Ando K, Suga N, Kingery WD. J Am Ceram Soc 1983;66:C130.
[39] Reed DJ, Wuensch BJ. J Am Ceram Soc 1980;63:88.